CNRS
Centre National de la Recherche Scientifique

INFN
Instituto Nazionale di Fisica Nucleare

Advanced Virgo calibration for O3: calibration based on free swinging Michelson

D. Estevez, B. Mours, L. Rolland, D.Verkindt

VIR-0529A-19

May 29, 2019

VIRGO * A joint CNRS-INFN Project
Project office: Traversa H di via Macerata - I-56021 S. Stefano a Macerata, Cascina (PI)
Secretariat: Telephone (39) 50 752 521 – Fax (39) 50 752 550 – e-mail virgo@pisa.infn.it

Contents

1 Introduction

The O3 LIGO-Virgo run started on April 1st, 2019, 15h UTC. Three types of calibration methods are being used or will be used for Virgo calibration, using independent length references: (i) the calibration based on free swinging Michelson technique, (ii) the calibration based on photon calibrators (PCal) and (iii) the calibration based on the Newtonian calibrators (NCal). This note describes the initial O3 calibration based on free swinging Michelson measurements, using the Virgo main laser wavelength as length etalon. Companion notes describes the modified timing distribution system, the detector calibration based on the PCals [**?**], the comparison of detector calibration from PCal and free Michelson [**?**], and the $h(t)$ reconstruction and uncertainty estimates of the initial online $h(t)$ [**?**]. The NCal method is not yet mature and the results from pre-O3 and O3 measurements will be analysed later.

The main goal of the calibration is to provide inputs for the $h(t)$ reconstruction algorithm, i.e. models for the mirror and marionette actuator responses, models for the interferometer output photodiode (B1) sensing and measurement of absolute timing.

The method for timing calibration of B1p sensing and the technic of free swinging Michelson calibration [1, 2], with the overall transfer procedure used to calibrate all mirror actuators have been already described for O2 calibration [3, 4, 5, 6].

Between O2 and O3, different hardware modifications affecting the calibration were done:

- the arm cavity payloads have been dismounted to replace the metallic wires with fused silica monolithic fibers, and some modifications have been done on the digital computation of the mirror and marionette DSPs. The actuator responses are expected to be similar to the O2 responses following these modifications, but all of them had to be measured again.
- the Virgo timing distribution has been upgraded to fulfill stronger phase noise requirements following the use of the digitally demodulated signals at 56 MHz for the interferometer control. It will be described in another note along with the new tools setup for O3 to monitor the timing stability. The basic idea is that instead of distributing the IRIG-B and 10 MHz clock from the main GPS receiver to all digital parts, a DaqBox timing mezzanine has been designed to regenerate the IRIG-B and build a 100 MHz clock distributed to the digital parts under vacuum, in particular to the DaqBoxes that acquire the B1 and B1p photodiode signals on SDB2 bench.
- the B1 and B1p photodiodes and pre-amp have been changed to be adapted to the reduction of impinging power (following reduction of DARM offset during commissioning) and to install high-quantum efficiency photodiodes on B1 for the squeezing.

Other modifications of the calibration were done to remove some sources of systematic uncertainty:

- when normalizing the measurement with the pendulum model, the frequency that is used to get the pendulum modulus and phase is exactly the frequency of the injected lines (while during O2 there was some offset related to the size of the bin): the injected frequencies and the lenght of the FFTs have been adjusted so that the injected frequencies is at the center of a FFT frequency bin.
- the different interferometer optical responses to input and end mirror motions have been taken into account (0.37% difference in modulus and 10 µs in phase).
- other modifications worth to be given??

In this note, emphasis is put on the calibration of B1p photodiode readout calibration (section **??**), since we will see that the DC response is not flat in frequency as initially assumed. This is the main change in the calibration compared to O2, and it introduced new systematic errors when using the free swinging Michelson technique.

Then, the overall calibration procedure (section 3) is reminded. In section 4, the NI and WI mirror actuation responses extracted by the free swinging Michelson technique but using two different reference photodiodes are shown and compared, and the stability of the measurement as afunction of time is studied. In section 5, the final calibration output, i.e. the BS and end mirror actuation responses and models useful for h(t) reconstruction are summarized and, in section 6, the models useful for hardware injections are given.

Finally, the timing calibration of the B1 photodiode sensing is described in section 7, using the same technique as described in [5].

The data used for the actuator calibration described in this note is from March 16th to 29th, 2019 (GPS period 1236750000 to 1237900000).

2 Calibration of B1p photodiode readout

The B1p beam is pick-off at the output of the interferometer before the output-mode cleaner cavity. It is used for calibration based on free swinging Michelson measurements, therefore its readout needs to be known.

2.1 B1p photodiode readout synoptic

Two photodiodes are being used to measure the B1p beam, called B1p_PD1 and B1p_PD2, B1p_PD1 receiving ten times more power than B1p_PD2. As a reminder, as shown in figure 1, the preamplifier of the photodiodes generates three outputs [5]:

- the DC output goes from 0 to tens of kHz. It allows to measure the full signal dynamic of the signal.

- the Audio output is high-passed at a few Hz, and goes up to about 100 kHz. Removing the DC part allows to measure the signal with low-noise in the band 10 Hz to 100 kHz.
- the RF output to acquire the signal in the band 1 MHz to more than 100 MHz that is demodulated digitally.

The synoptic of the B1p readout is shown on figure 1. It is similar to the one from O2 except that some modifications were done on the preamplifier filters as described in the next section. Another modification was done at the level of the real-time Acl process: as during O2, the DC and Audio channels are sent out at 100 kHz from the ADC channel; but they are now directly low-pass filtered and decimated down to 10 kHz to generate the channels called SDB2_CAL_B1p_B1_DC_10kHz (for PD1 and PD2, and DC and Audio). The demodulated RF channels (called I and Q) are still sampled at 10 kHz as during O2.

During O2, the DC and Audio output channels were sampled at 20 kHz while the demodulated channels were sampled at 10 kHz. As a consequence, extra offline filter/decimation down to 10 kHz was needed on the DC and Audio channel before doing ΔL reconstruction on free swinging Michelson data. Moreover readout timing was not measured directly on these channels. For O3, having all channels (DC, Audio, I and Q) sampled at 10 kHz from the front-end removes possible errors/oversights in the calibration procedure.

2.2 Hardware modification of B1p readout between O2 and O3

With the increase of input power between O2 and O3, the B1p_PD1 Audio channel was saturating during free swinging Michelson measurements, and due to coupling with the DC channel, it was generating glitches in the DC channel. As a consequence, it could not be used any more for calibration. In order to fix this, the high-pass filter of the Audio channel was moved from 2 Hz to 16 Hz. It indeed fixed the saturation issue, but also showed up an effect that was not taken into account before: contrary to what was assumed earlier, the response of the DC channel is not flat in frequency. Due to couplings between the Audio and DC channels, the impedance of the DC channel depends on frequency around the Audio high-pass filter (around a few hertz).

2.3 Measurements of B1p DC response shape with a LED

Dedicate measurements were setup to estimate the non-flat response and take it into account in the calibration procedure: an excitation was sent to a LED placed in front of the photodiode as shown in figure 2(c). This measurement requires the SDB2 vacuum tank to be opened to access the bench and bring the LED on the bench close to the photodiode, leading to scarse measurements (only twice in January and March 2019). As another drawback of this measurement, the temperature of the photodiode and preamplifier decreases when the vacuum tank is opened: hence the measurement is done at temperature ($\sim 38°$C) lower than in standard

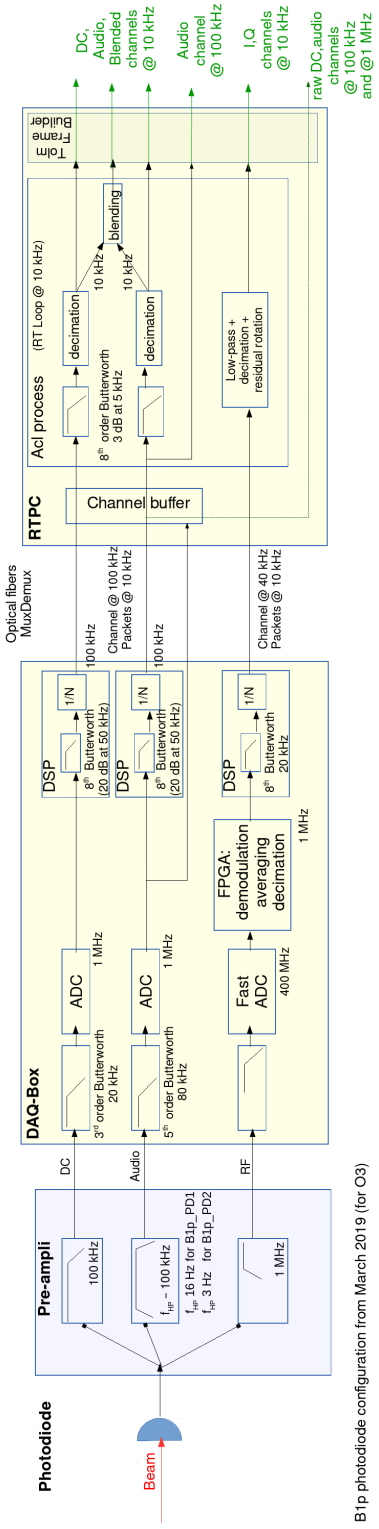

Figure 1: Sketch of the B1p sensing at the start of O3.

condition (~ 53°C), leading to systematic errors since the frequency-dependent shape depends on temperature.

On January 18th (logbook 44428), the measurement was done with the photodiodes at ~ 38°C (the vacuum tank was opened since more than 2 hours), injecting lines for tens of minutes with the LED. It leads to precise measurement of the frequency response fit by a pole and a zero, as shown in figures 2(a) and 2(b). In order to check the temperature dependence, another measurement was done on March 14th (logbook 45259), injecting lines for few minutes with the LED soon after the vacuum tank was opened, hence during the cool-down. This could only be done on one photodiode, choosen to be B1p_PD1. Analysing the data by chunks of minutes gave only rough measurements of the pole and zero as a function of temperature.

2.4 Measurements of B1p DC response shapes during free swinging Michelson data

In order to estimate the pole and zero frequencies at the nominal temperature of ~ 53°C, the transfer function of B1p_PD2_DC/B1p_PD1_DC has been measured during free swinging Michelson measurements (using February 15th data, logbook 45259). Since both photodiodes receive the same beam, they show coherence and the transfer function shows two poles and two zeros as shown in figure 2(d).

2.5 Estimation of B1p DC response shape vs temperature

From the different measurements of the pole and zero estimated at different frequencies, the temperature dependence has been estimated as shown on figures 2(e) and 3(a).

2.6 Whitening of the B1p DC response

On March 14th 2019, the B1p_PD1,2_DC channels have been whitened using the pole and zero frequencies[1] estimated at 53°C.

2.7 Effect of non-flat DC response on free swinging Michelson analysis

The figure 4 illustrates the effect of the non-flat DC response of B1_PD1: the ΔL reconstruction has been run using the raw (not whitened) channel. It directly modifies the shape of the

[1] The following frequencies have been setup in the SDB2_Photodiode process configuration:
PD1: zero at 10.285 Hz and pole at 16.068 Hz.
PD2: zero at 1.57 Hz and pole at 1.8857 Hz.

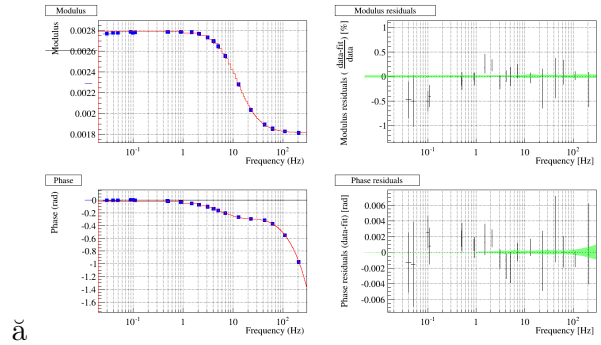

ă

(a) B1p_PD1_DC vs LED excitation (Jan 14th, 38°C)

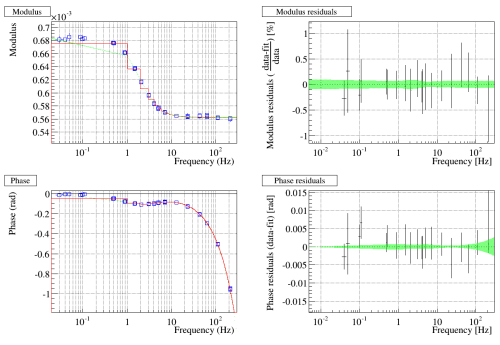

ă

(b) B1p_PD2_DC vs LED excitation (Jan 14th, 38°C)

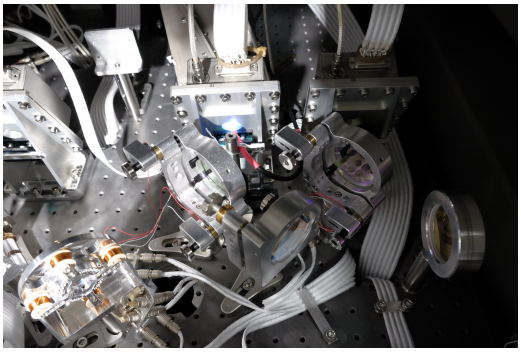

(c) LED placed in front of photodiode

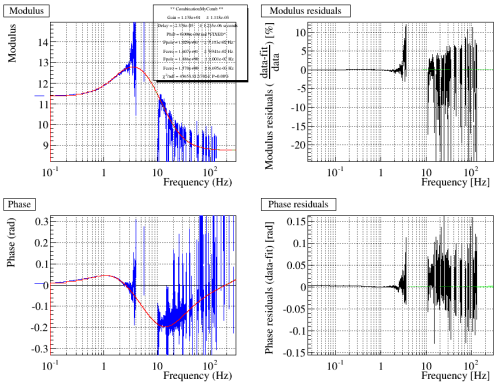

(d) Transfer function PD2_DC/PD1_DC (Feb 15th, 53°C)

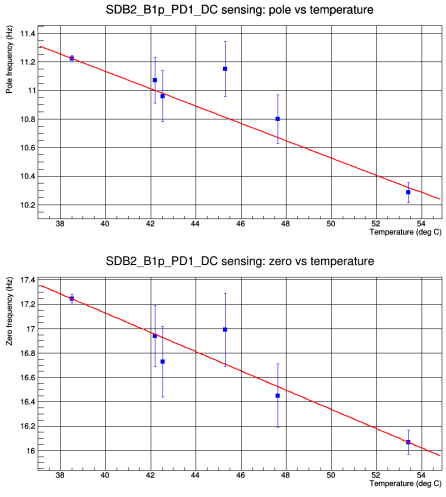

(e) B1p_PD1_DC: pole and zero vs frequency

Figure 2: Summary of the measurements for the B1p PD1 DC frequency-dependent shape as function of temperature. First line shows the measurements on PD1 and PD2 made with the LED long excitations (blue), the pole-zero fit (red line) and the fit residuals on the right panels. The green area indicates the 1-sigma statistical uncertainties of the fit. Figure c is a picture of the LED measurement. Figure d shows the comparison of PD1 and PD2 response done via their transfer function (only points with coherence higher than 90% are shown).

reconstructed actuation response, whose shape is expected to be a simple pole around 300 Hz as shown by the red curve.

3 Overview of the actuator calibration procedure

The calibration of the different actuators cannot be done in a single measurement. The different steps of overall procedure are shown in figure 5. They are the same as during O2. More details about the measurements themselves can be found in the O2 notes [5, 6].

4 Calibration of NI, WI, BS mirror actuators: free swinging Michelson

The first step of the calibration is the measurement of the NI, WI and BS mirror actuators responses in free swinging short Michelson data, using the laser wavelength as length etalon: 1064.0 ± 0.1 nm. They are measured in the range 10 Hz to 1 kHz.

Since B1p_PD1 receives ten times more power than B1p_PD2 photodiode, the better photodiode to be used for free swinging Michelson calibration sensitivity is PD1, and it indeed provides lower statistical uncertainties and allows to measure actuation response up to 1 kHz while PD2 measurements are less precise and limited to below a kHz.

Using PD1 has however a drawback with respect to using PD2: since the whitening filter of PD1 has pole and zero close to 10 Hz and 16 Hz, errors on the knowledge of the whitening filter generate fake frequency-dependent shape between 10 Hz and about 30 Hz in the actuation response measured. In the case of PD2 whitening filter errors, since the pole and zero are around 2 Hz, the effect is not seen above 10 Hz.

However, in both cases, the absolute value of the measured modulus has systematic uncertainties coming from the imperfect compensation of the pole and zero with the whitening filter.

In this section, we first show the results of NI mirror actuation response measured using both PD1 and PD2 photodiodes and we then compare them.

4.1 Measured NI actuator response with B1p_PD1 and B1p_PD2

The actuator response of NI in high-power (HP) mode as measured using the whitened PD1_DC and PD2_DC channels is shown on figure 6 (normalized by the simple pendulum model as usual). It has been fit with a simple pole function and a delay, shown in red on top of the blue data points.

As stated above the statistical errors are lower when using PD1. Below 30 Hz, the measure shape is flat when using PD2 while some structure is seen when using PD1, with a modulus variation of 1%. Also on the phase, some structure with phase shift up to 5 mrad is seen at low frequency when using PD1 photodiode. This indicates that the whitening filter of PD1 does not perfectly compensate for the pole and zero discussed in previous section. As a consequence, when using PD1, the range of the fit has been limited to 30 Hz to few kHz to be insensitive to the low frequency bias.

The DC gains of the fit, given in the figure legends, significantly differs by $1.2\% \pm 0.1\%$.

The figure 7 shows the same comparison for the WI mirror actuation.

4.2 Study of the measurement stability vs time

During O3 calibration excitation periods, we have added, for every excited actuator, a line around 75 Hz which is present in all dataset. It permits following closely the time stability of the measurements.

Figure 8 shows the NI actuation reponse modulus and phase measured at 78.2 Hz in March 2019, over the full period, and over each of the three calibration periods. The chi2 probability of the fit of the modulus by a constant is very low, pointing out that the measurement is not constant in time. In order to estimate systematic uncertainties, the error bars of the data points have been increased up to reaching a χ^2 probability of 5%. The results are shown on figure 10. On the modulus, up to 300 Hz, uncertainties are of the order of 0.5%, dominated by systematic uncertainties associated to time variation ; at higher frequency, statistical uncertainties increase, up to 2% at 1300 Hz, and hide any small time variation. On the phase, no time variation are seen on top of the statistical uncertainties, which are of the order of 1 mrad up to 200 Hz and up to 20 mrad at 1 kHz.

The figure 11 shows the time variation of the measurements when using PD2. In this case the data are compatible with being constant with time, with statistical uncertainties of the order of 0.3% in modulus and 3 mrad in phase below 100 Hz.

A probable origin of the higher time variation when using PD1 are the variations of the DC response shape, which is then not properly compensated by the fixed whitening filter. Even limiting the fit to above 30 Hz, the incorrect pole-zero correction has indeed an effect on the B1p PD1 amplitude value, but not on the phase.

5 Calibration of NE, WE and BS mirror actuators for HRec

The actuation models used for the h(t) reconstruction are the responses from the channels Sc_MIR_Z_CORR, timestamped as stored in the Virgo raw data, to the mirror motion ΔL at a given GPS time.

The BS mirror actuator is calibrated directly in low-noise 1 (LN1) mode from the free swinging Michelson data. The response function, estimated using B1p PD1 and PD2 respectively, is shown in figure 13(a) and 14(a).

Following the calibration procedure, the NI (resp. WI) mirror actuator response measured with the free swinging Michelson technique is then transferred to the NE (resp. WE) mirror actuator response in low-noise 2 (LN2), using excitations while the interferometer is locked, but with the NI and WI actuators kept in high-power mode (instead of being opened during standard lock state). The figures **??** and **??** show the raw response functions for NE based on using PD1 and PD2 respectively for the free swinging Michelson data analysis (resp. figures **??** and **??** for WE). They are obtained by multiplying the NI (resp. WI) raw response from free swinging Michelson data with the raw ratio of NE and NI (resp. WE and WI) transfer functions.

For comparison, the ratio of the response functions estimated using PD1 and PD2 are shown in appendix A.

The calibrated mirror actuation response models, based on using B1p PD1 for free swinging Michelson analysis, are reported in table 1. They give the transfer function from the $Sc\_NE, WE, BS\_MIR\_Z\_CORR$ channels as measured in Virgo raw data to the mirror motion ΔL in absolute GPS time.

They are derived from the raw measurements and fit, with the following corrections applied:

- subtraction of the delay of the B1p photodiode readout electronics: 175 µs(that includes the 16 µs timestamp offset from absolute GPS time), see section 7.
- for NE and WE, addition of the 10 µs delay coming from the different arm cavity optical responses to input and end mirror motions.
- for NE and WE, the raw gain is multiplied by 0.9963 since the arm cavity optical responses to end mirror motion is higher by 0.37% than the one to input mirror motion.

Model		Mirror actuators			
Type	parameters	NE in LN2	WE in LN2	BS in LN1	PR in HP
Gain (µm/V)		0.4957 ± 0.002	0.4122 ± 0.0019	1.09176 ± 0.00038	±
Delay (µs)		-169.5 ± 1.5	-168.5 ± 1.6	391.3 ± 1.7	±
Extra-delay for HRec (µs)		10	10	0	0
1st order pole	f_p (Hz)	114.2 ± 23	102.4 ± 35.8	–	±
1st order zero	f_0 (Hz)	119.1 ± 24	104.0 ± 36.2	–	–
1st order pole	f_p (Hz)	—		–	–
1st order zero	f_0 (Hz)	—		–	–
2nd order zero	f_0 (Hz)	–	–	654.2 ± 6	–
	Q	–	–	0.6577 ± 0.0034	–
2nd order zero	f_0 (Hz)	–	–	1222.7 ± 5	–
	Q	–	–	1.586 ± 0.027	–
simple pendulum	f_p (Hz)		0.6		–
	Q		1000		

Table 1: Summary of the mirror actuator calibration models useful for h(t) reconstruction, based on the free swinging Michelson data using B1p PD1 as reference photodiode. Without the extra-delay, responses are from Sc_MIR_Z_CORR channels to the induced mirror motion in absolute GPS time. With the extra-delay, responses are from Sc_MIR_Z_CORR channels to the induced h(t) in absolute GPS time. Only statistical errors are reported here. The extra-delay reported here is a delay to be added in HRec configuration to take into account that the arm cavity optical response cannot be approximated by only simple pole as assumed in HRec, but has some delay in the case of end mirror motion The models are valid between 10 Hz and 1.5 kHz.

6 Calibration of NE, WE mirror actuators for hardware injections

It is possible to inject external $h(t)$ signal in the interferomter via the NE and WE mirror electromagnetic actuators. The excitation signals are stored in the Virgo raw data called CAL_NE_MIR_Z_NOISE (resp. WE). The transfer functions from these channels, timestamped as stored in the Virgo raw data, to the mirror motion ΔL at a given GPS time are summarized in table 2. They are the same as the ones given in previous section, but with a different delay and an additional filter that describes the analog computation between CAL_MIR_Z_NOISE and Sc_MIR_Z_CORR channels in the suspension DSPs: channel extension from 10 kHz to 40 kHz, Chebyshev filtering and decimation from 40 kHz to 10 kHz. This is approximated by two simple poles at 8174 Hz and a delay of 412.5 µs. As shown in figure 15, this approximation is valid up to 1 kHz within 0.05% in modulus and 1.5 µs in phase.

The extra-delay given in the last line of the table must be added to get the response from the excitation channel CAL_MIR_Z_NOISE to the generated $h(t)$. Indeed, the optical response of the interferometer to gravitational waves and to end mirror motions are similar but differ by a delay of 10 µs for the Virgo arm length.

Model		Mirror actuators	
Type	parameters	NE in LN2	WE in LN2
Gain (μm/V)		0.4957 ± 0.002	0.4122 ± 0.0019
Delay (μs)		$+243.0 \pm 1.5$	$+244.0 \pm 1.6$
1st order pole	f_p (Hz)	114.2 ± 23	102.4 ± 35.8
1st order zero	f_0 (Hz)	119.1 ± 24	104.0 ± 36.2
1st order pole	f_p (Hz)	8174	
1st order pole	f_p (Hz)	8174	
simple pendulum	f_p (Hz)	0.6	
	Q	1000	
Extra-delay for HI (μs)		10	10

Table 2: Summary of the mirror actuator calibration models useful for inducing known external excitation in the interferometer, based on free swinging Michelson data using B1p PD1 as reference photodiode. Without the extra-delay, responses are from CAL_MIR_Z_NOISE channels to mirror motion in absolute GPS time. With the extra-delay, responses are from CAL_MIR_Z_NOISE channels to induced $h(t)$ in absolute GPS time. Only statistical errors are reported here. The models are valid between 10 Hz and 1 kHz.

7 Timing calibration of the B1p DC and Blended channels

7.1 Timing of B1p PD1

The channel used for the free swinging Michelson reconstruction is V1:SDB2_CAL_B1p_PD1_Blended_10kHz. We need to know the delay of the sensing of this channel to take it into account in the actuator calibration procedure.

The timing of B1p PD1 photodiode is estimated in three steps:

1. measure the delay of the Audio raw channel sampled at 1 MHz during specific data when the IRIG-B signal from the main GPS receiver is directly sent in front of the photodiode via a LED. This is done looking at the time series of the channel.

2. measure the delay from the Audio channel sampled at 1 MHz to the Audio channel reduced at 10 kHz.

3. measure the delay from the Audio channel to the Blended channel, both sampled at 10 kHz.

Step 1: delay of the Audio raw channel sampled at 1 MHz – Figure 16 shows the time series of the channel V1:SDB2_B1p_PD1_Audio_raw_1MHz_DS sampled at 1 MHz while the IRIG-B signal was flashed using a LED put in front of the photodiode on the bench. The cable from the GPS receiver to the LED was 20 m long, inducing a negligible delay.

The position of the 1 PPS edge of the IRIG-B signal in the channel as stored in the Virgo frames is at $-11 \pm 1.5\,\mu$s. It corresponds to the expected position, with -16 µs coming from the Virgo data timestamp offset due to the timing distribution, and +5 µs delay in the photodiode sensing chain (coming from the analog anti-alias filter before the ADC).

This was measured on specific measurements made on March 12th 2019 (GPS 1236423160).

Step 2: delay from the 1 MHz to the 10 kHz Audio channels – Figure 17 shows the measured transfer function from V1:SDB2_B1p_PD1_Audio_raw_1MHz_DS to ă V1:SDB2_CAL_B1p_PD1_Audio_10kHz. The phase has been fit between 10 Hz and 2 kHz and matches a delay of 186 µs, within better than 1 µs as validated from the residuals.

Step 3: delay from the 10 kHz Audio to Blended channels – In order to have coherence between the two channels, the transfer function from V1:SDB2_CAL_B1p_PD1_Audio_10kHz to V1:SDB2_CAL_B1p_PD1_Blended_10kHz has been computed during free swinging Michelson measurements. The figure 18 shows the transfer function: at high frequency, the phase converges to π, which is consistent with no delay between the two channels but only a sign flip

7.2 Timing of B1p PD2

The transfer functions from V1:SDB2_CAL_B1p_PD1_Audio_10kHz to V1:SDB2_CAL_B1p_PD2_Audi
and from V1:SDB2_CAL_B1p_PD1_Blended_10kHz to V1:SDB2_CAL_B1p_PD2_Blended_10kHz have been computed on free swinging Michelson data with excitations up to 1.8 kHz. Around the excitation lines,there is a coherence higher than 97% between the channels and the phase of the transfer functions is compatible with 0. It confirms that the delay of B1p PD2 sensing is the same as the one of B1p PD1 sensing.

7.3 Summary

From the measurements, one can conclude that the sensing delay of the channels V1:SDB2_CAL_B1p_PD1_
and V1:SDB2_CAL_B1p_PD2_Blended_10kHz is 175 $\pm$ 2.5 µs. Correcting for this delay corrects for both the readout delay and the timestamp offset of the Virgo data.

Photodiode channel	$SDB2\_CAL\_B1p\_PD1\_Blended$ and $SDB2\_CAL\_B1p\_PD2\_Blended$
Measured delay (µs)	175 ± 2.5 µs

Table 3: Summary of the delay from power arriving on the B1p photodiode at a given GPS time to the photodiode channel stored in the Virgo frames.

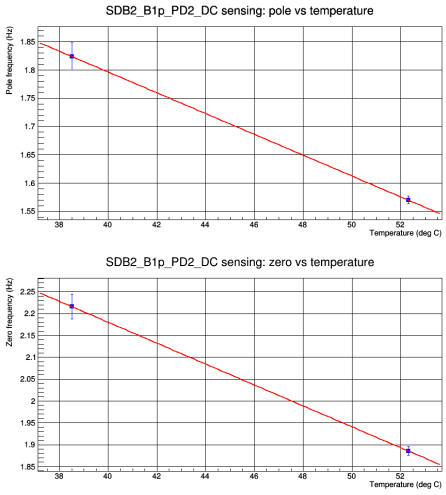

(a) B1p_PD2_DC:
pole and zero vs frequency

Figure 3: Summary of the measurements for the B1p PD2 DC frequency-dependent shape as function of temperature. It shows the estimated temperature dependence of the poles and zeros for the PD1 and PD2 photodiode DC responses.

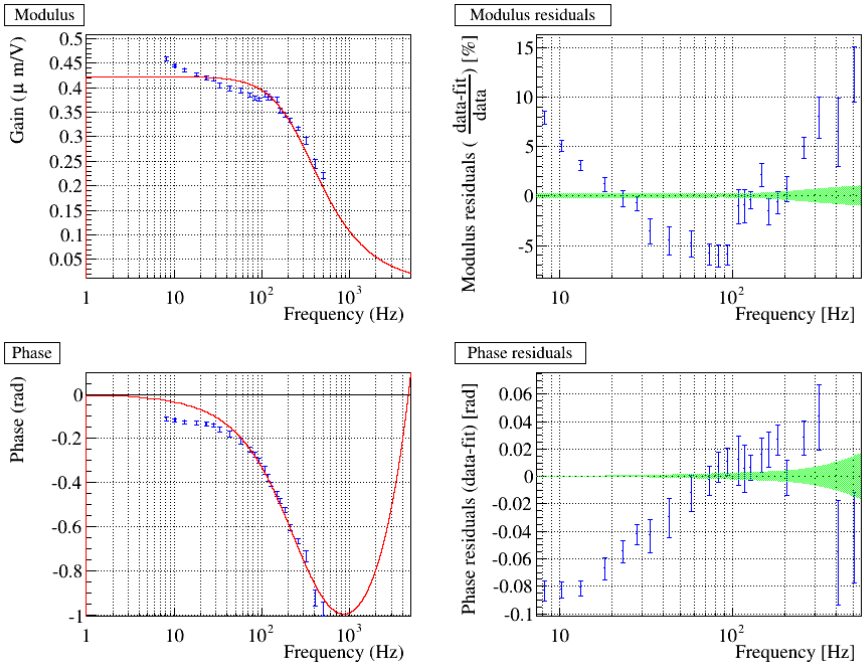

Figure 4: NI mirror actuator response reconstructed without whitening the DC response of B1p_PD1_DC.

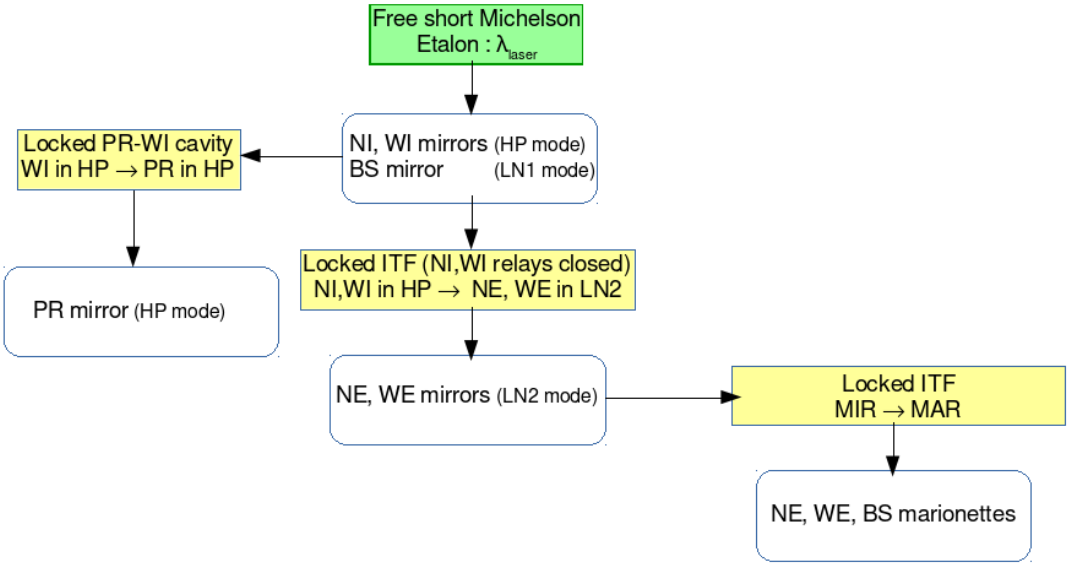

Figure 5: Overview of the mirror and marionette calibration procedure. The filled areas indicate the types of measurements while the empty areas indicate the calibrated actuators.

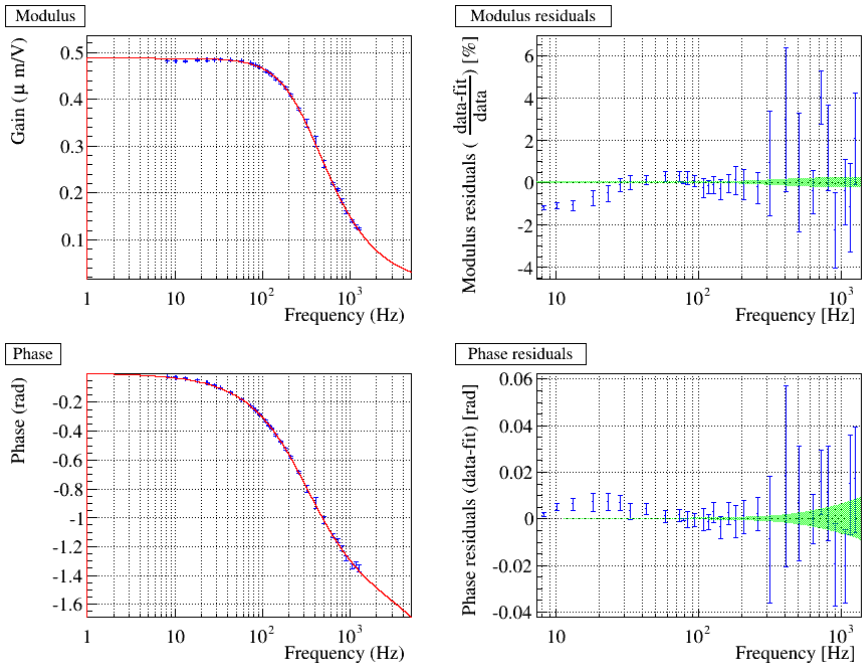

(a) PD1 (whitened)$Gain = 0.48728 \pm 0.00020$ μm/V, $f_{pole} = 322.0 \pm 0.9$ Hz

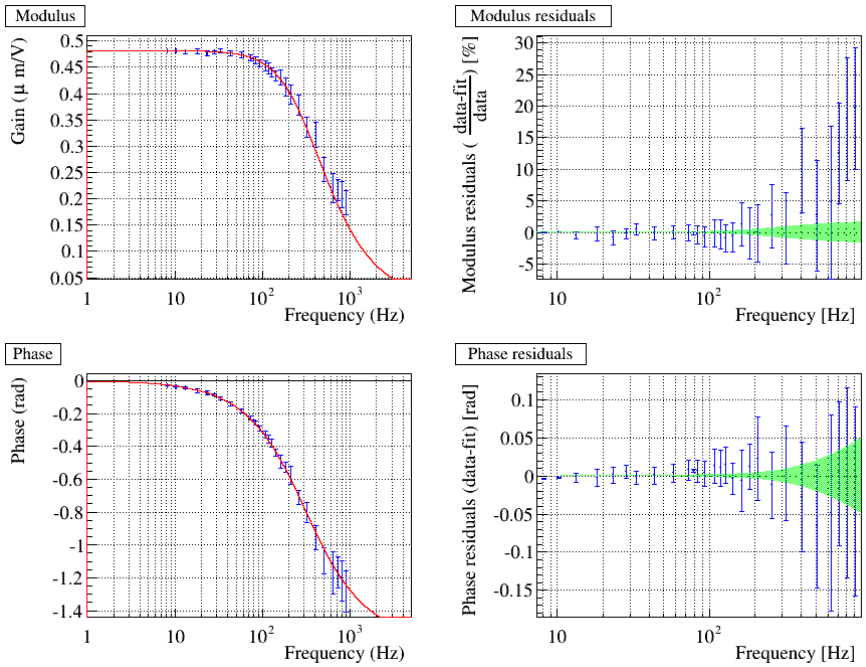

(b) PD2 (whitened)$Gain = 0.48165 \pm 0.00020$ μm/V, $f_{pole} = 307.2 \pm 5.6$ Hz

Figure 6: NI mirror actuation response (normalized by a simple pendulum response) as measured using the whitened B1p PD1 and PD2 photodiodes. On the right panels, the fit residuals are shown. The greenish area indicate the fit statistical uncertainties.

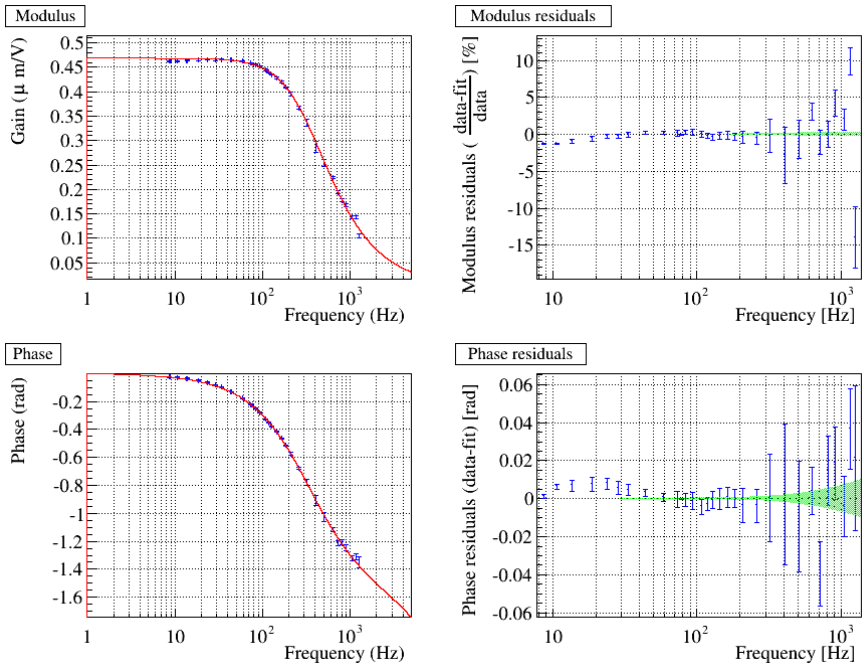

(a) PD1 (whitened)

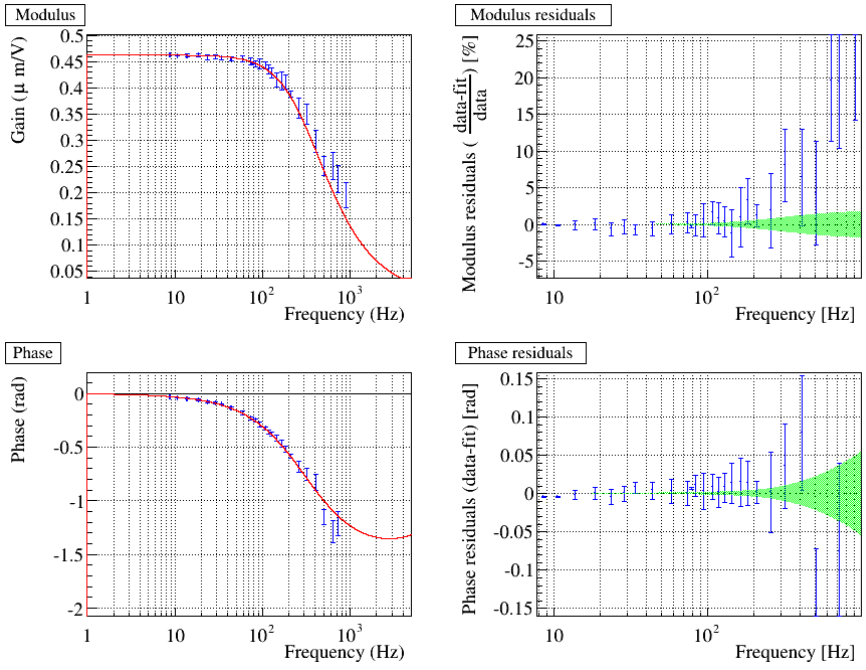

(b) PD2 (whitened)

Figure 7: WI mirror actuation response (normalized by a simple pendulum response) as measured using the whitened B1p PD1 and PD2 photodiodes;

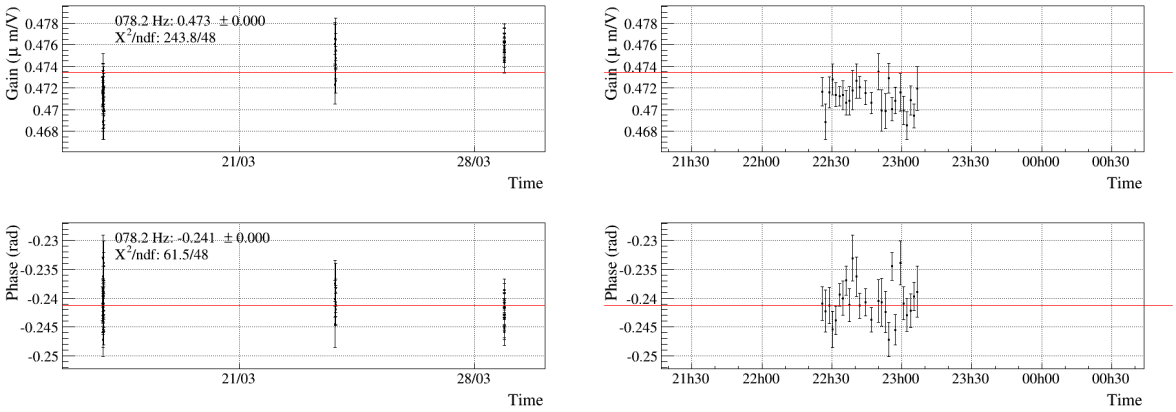

(a) NI, using PD1: all

(b) NI, using PD1: zoom on day 1

(c) NI, using PD1: zoom on day 2

(d) NI, using PD1: zoom on day 3

Figure 8: NI mirror actuation response measured at 78.2 Hz in every dataset, using B1p PD1.

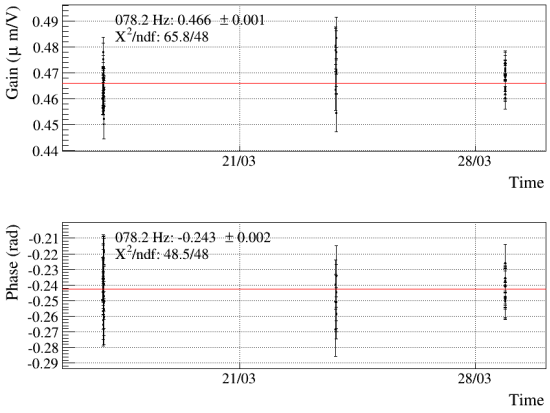

(a) NI, using PD2: all

Figure 9: NI mirror actuation response measured at 78.2 Hz in every dataset, using B1p PD2.

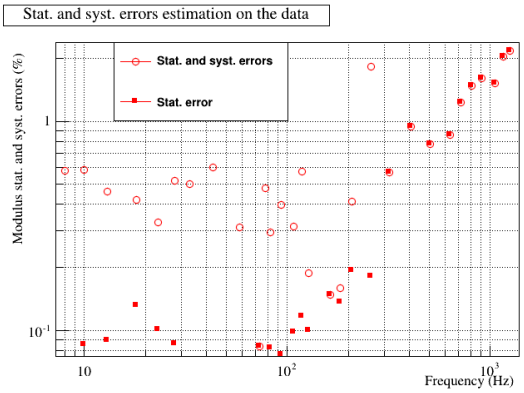

(a) NI, using PD1: modulus uncertainties

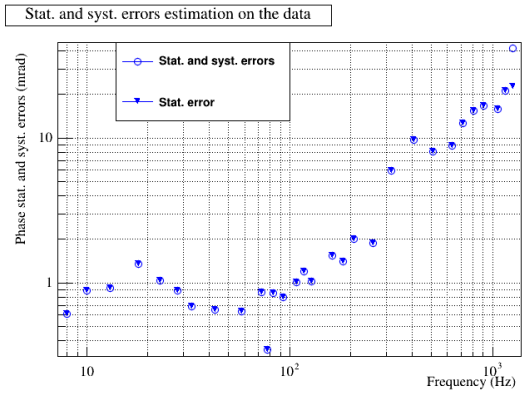

(b) NI, using PD1: phase uncertainties

Figure 10: Summary of 1 σ statistical uncertainties (filled markers) and estimation of the sum of statistical and systematic uncertainties (empty markers) so that the hypothesis of a constant value is true at the 5% level.

Figure 11: NI mirror actuation response measured at 78.2 Hz in every dataset.

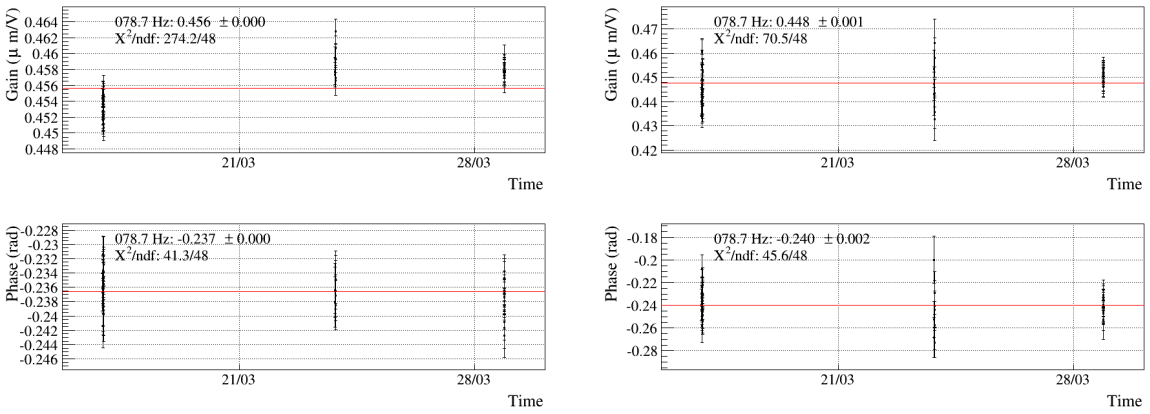

(a) WI, using PD1: all

(b) WI, using PD2: all

Figure 12: WI mirror actuation response measured at 78.7 Hz in every dataset, with either B1p PD1 or PD2 photodiode.

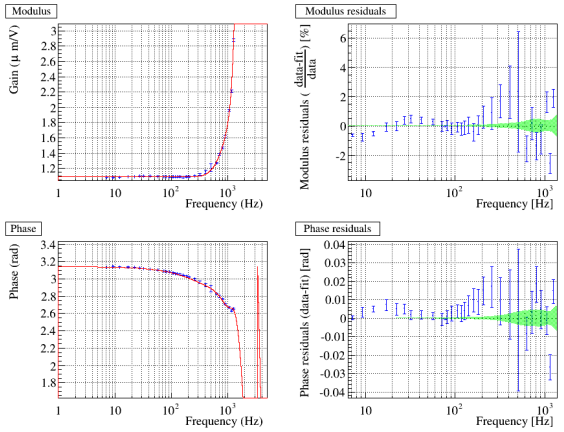

(a) BS, using B1p PD1

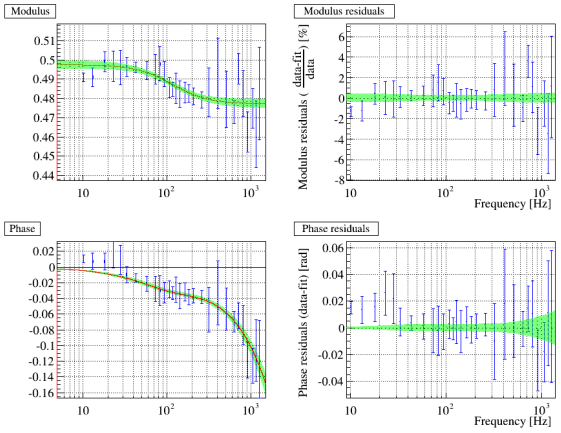

(b) NE, using B1p PD1

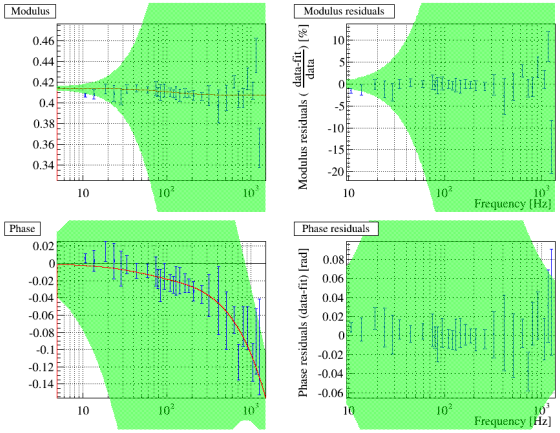

(c) WE, using B1p PD1

Figure 13: BS, NE and WE mirror actuation response measured by using free swinging Michelson data and B1p PD1 photodiode.

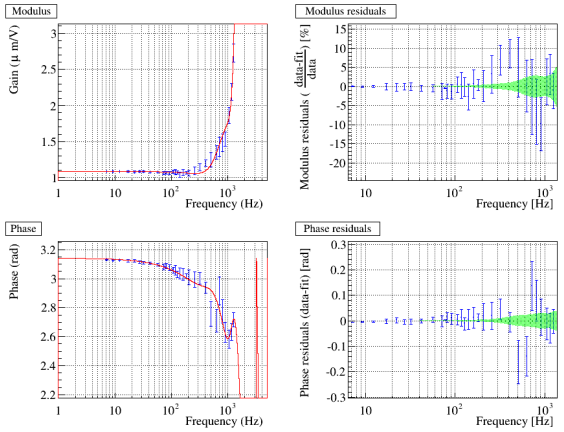

(a) BS, using B1p PD2

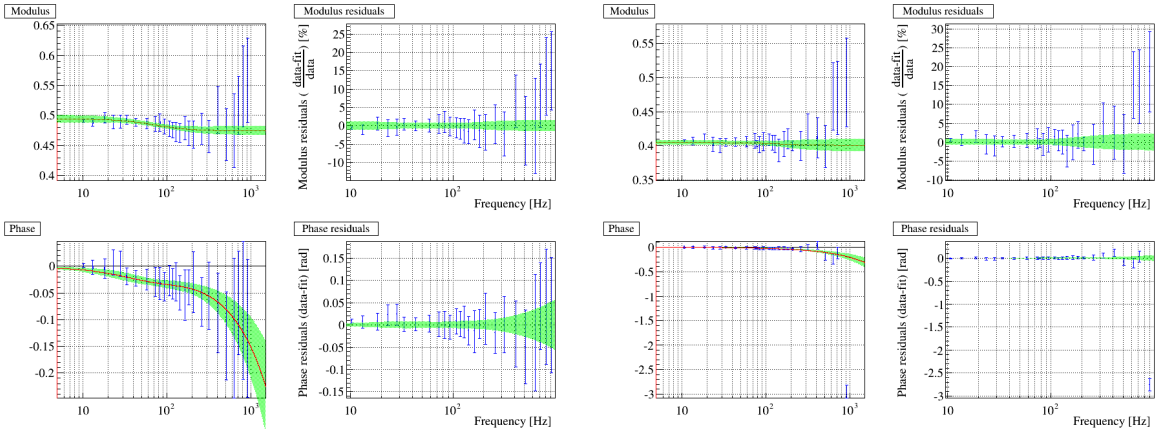

(b) NE, using B1p PD2

(c) WE, using B1p PD2

Figure 14: BS, NE and WE mirror actuation response measured by using free swinging Michelson data and B1p PD2 photodiode.

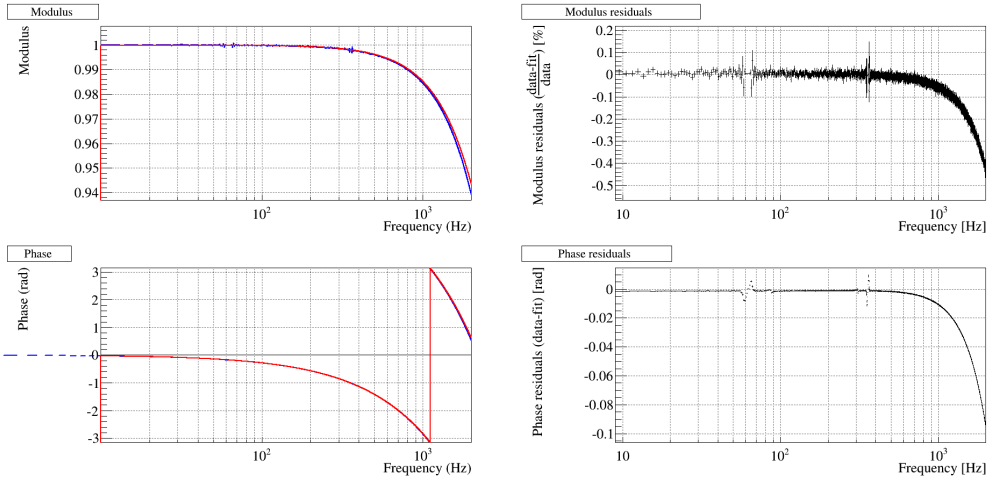

Figure 15: Transfer function from CAL_NE_MIR_Z_NOISE to Sc_NE_MIR_Z_CORR. The fit described in the text is shown in red. The right column gives the residuals of the modulus and phase fit. This is the same for all mirror actuators (NE, WE, BS, PR).

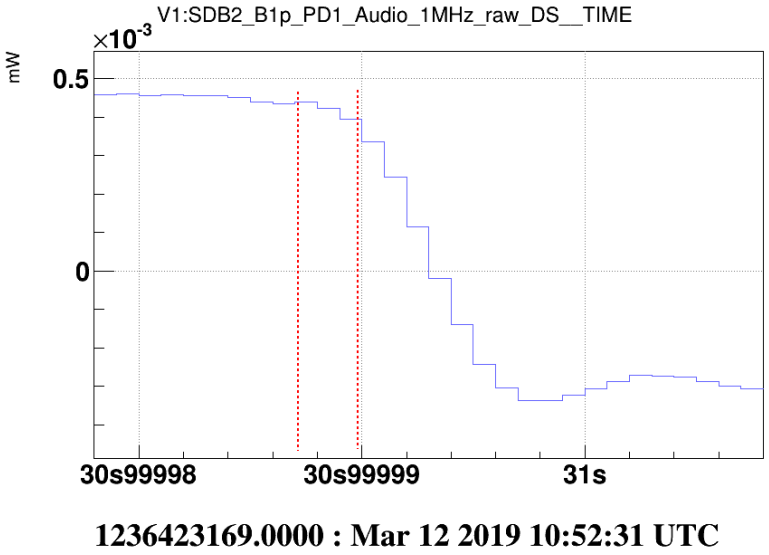

Figure 16: Times series of V1:SDB2_B1p_PD1_Audio_raw_1MHz_DS sampled at 1 MHz, zoomed around the 1 PPS of the IRIG-B (readout with a minus sign); The red dashed line indicate the estimated position of the rising edge as seen in the time series.

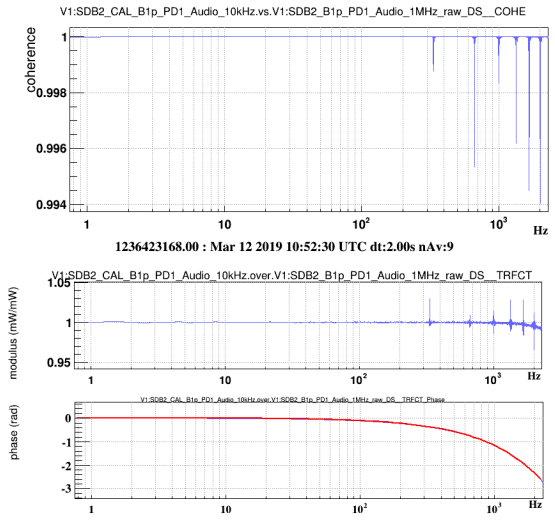

(a) Coherence and transfer function

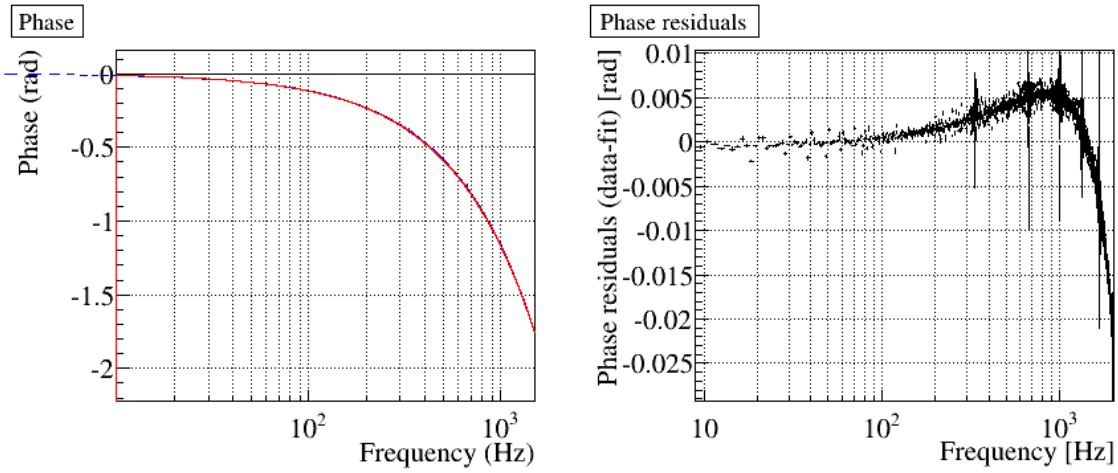

(b) Fit of the phase and residuals

Figure 17: Transfer function from V1:SDB2_B1p_PD1_Audio_raw_1MHz_DS to V1:SDB2_CAL_B1p_PD1_Audio_10kHz.

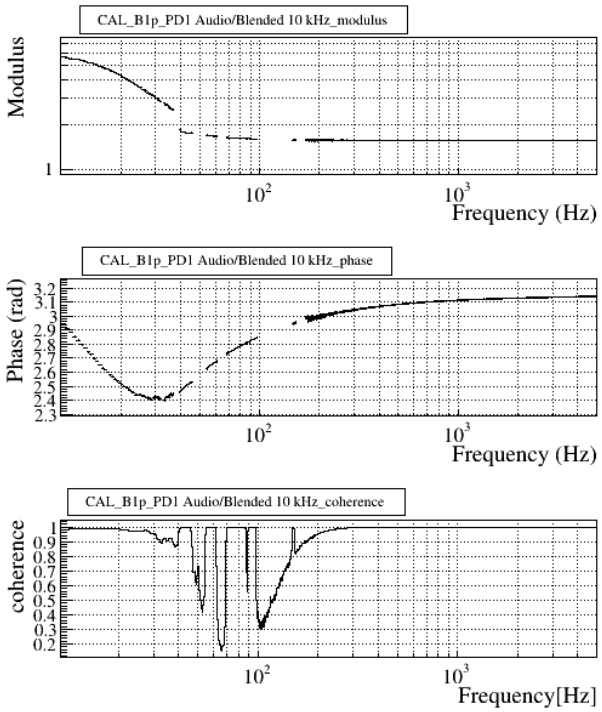

Figure 18: Transfer function from V1:SDB2_CAL_B1p_PD1_Audio_10kHz to V1:SDB2_CAL_B1p_PD1_DC_10kHz.

8 Conclusions

In this note, we have described the calibration of the Virgo mirror electromagnetic actuators at the start of the run O3 (1st April 2019) based on the free swinging Michelson technique. The data used for the actuator calibration is from before the start of the run, from March 16th to 29th, 2019 (GPS period 1236750000 to 1237900000).

As a new information compared to O2 calibration, we have shown that systematic uncertainties on the measurements come from the frequency dependence of the B1p photodiode DC readout, mainly below 30 Hz. Since, for O3, the two B1p photodiodes have different DC readout, we have compared the results using one or the other photodiode and found a difference of the order of 1% in modulus of the response functions.

Weekly measurements are being taken during O3. They will permit to reduce statistical uncertainties and, more importantly, to better study the systematic uncertainties as time variations. In particular, it may be possible to disentangle between fake variations coming from B1p sensing, which is currently the main culprit, or real variations of the actuator themselves.

The extracted mirror actuator models have been summarized for reference. Another note [**?**] is being written to compare these responses with the responses estimated using the photon calibration technique [7].

The systematic errors from B1p readout not being precisely controlled, it reduces our confidence in using the free swinging Michelson technique for a percent level calibration. As a consequence, since the start of O3, the response functions used in the online h(t) reconstruction are no more the ones extracted from the free swinging Michelson and described in this note, but are the ones extracted from the photon calibration.

References

[1] L. Rolland *et al.*, "Mirror motion reconstruction for free swinging Michelson data," *Virgo note*, vol. VIR-0112A-08, Nov. 2008.

[2] L. Rolland, "Free Michelson calibration for Advanced Virgo," *Virgo note*, vol. VIR-0119A-13, Apr. 2013.

[3] D. Estevez, L. Rolland, *et al.*, "Advanced Virgo SDB2_B1/B1p Timing for O2," *Virgo note*, vol. VIR-0773A-17, Oct. 2017.

[4] B. Mours, L. Rolland, *et al.*, "Check of the DAQ timing during O2," *Virgo note*, vol. VIR-0708B-17, Sept. 2017.

[5] L. Rolland *et al.*, "Advanced Virgo calibration for O2: photodiode sensing and mirror and marionette actuator responses," *Virgo note*, vol. VIR-0707C-17, Sept. 2017.

[6] L. Rolland *et al.*, "Advanced virgo calibration for o2: update for h(t) reconstruction reprocessing v1o2repro2a," *Virgo note*, vol. VIR-0013B-18, Jan. 2018.

[7] E. Estevez, L. Rolland, *et al.*, "Calibrating end mirror and marionette actuators with photon calibrators at the beginning of o3," *Virgo note*, vol. VIR-0466A-19, May 2019.

A Comparison of NE and WE actuator responses estimated using B1p PD1 and PD2

The following figures show the comparison of the NE and WE actuator responses estimated in free swinging Michelson but using either B1p PD1 or PD2 photodiode for the ΔL reconstruction.

The non-flat shape of the transfer function ratio is coming from slightly different values of fit poles and zeros on the different reconstructed data.

The gain value is estimated with statistical uncertainties of 0.4% and 0.7% respectively when using PD1 or PD2. There is a systematic slight over-estimation of the gain when using PD1 compared to PD2, by 1% to 2%.

The delay is fit with an uncertainty of the order 1µs when using PD1, and 10µs when using PD2 (since PD2 receives less power than PD1). Hence, the differences of 8 and 16µs when comparing the models obtained from PD1 and PD2 are consistent with the statistical errors of the fit.

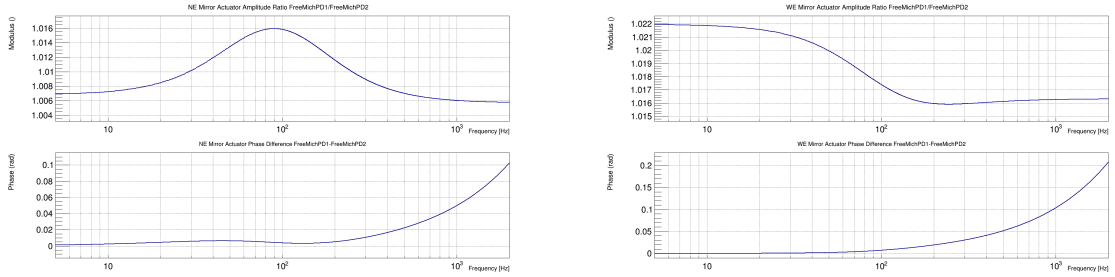

(a) NE (b) WE

Figure 19: NE and WE mirror actuation response measured based on free swinging Michelson data and using B1p PD1 photodiode.

B Temperature monitoring of B1p PD1 and PD2 photodiodes during free swinging Michelson measurements

The figure 20 shows the time series of the temperature monitoring of the B1p photodiodes during 8 different free swinging Michelson measurements in March and April 2019.

During a measurement, the temperature of PD2 is stable while the temperature of PD1 increases, by about 0.2°C in about 15 minutes. This can be explained since the shutter of PD2 is opened already before the measurement while the shutter of PD1 is opened only at the beginning of the measurement.

From one measurement period to another one, the temperature varies by 0.3°C.

Such temperature variations induce variations in the analog electronics of the DC and Audio channels, and probably change the shape of their response. More detailed analysis of the data must be one to understand wether such variations induce significant mistuning of the whitening filter used for the DC channels, and of the blending filters.

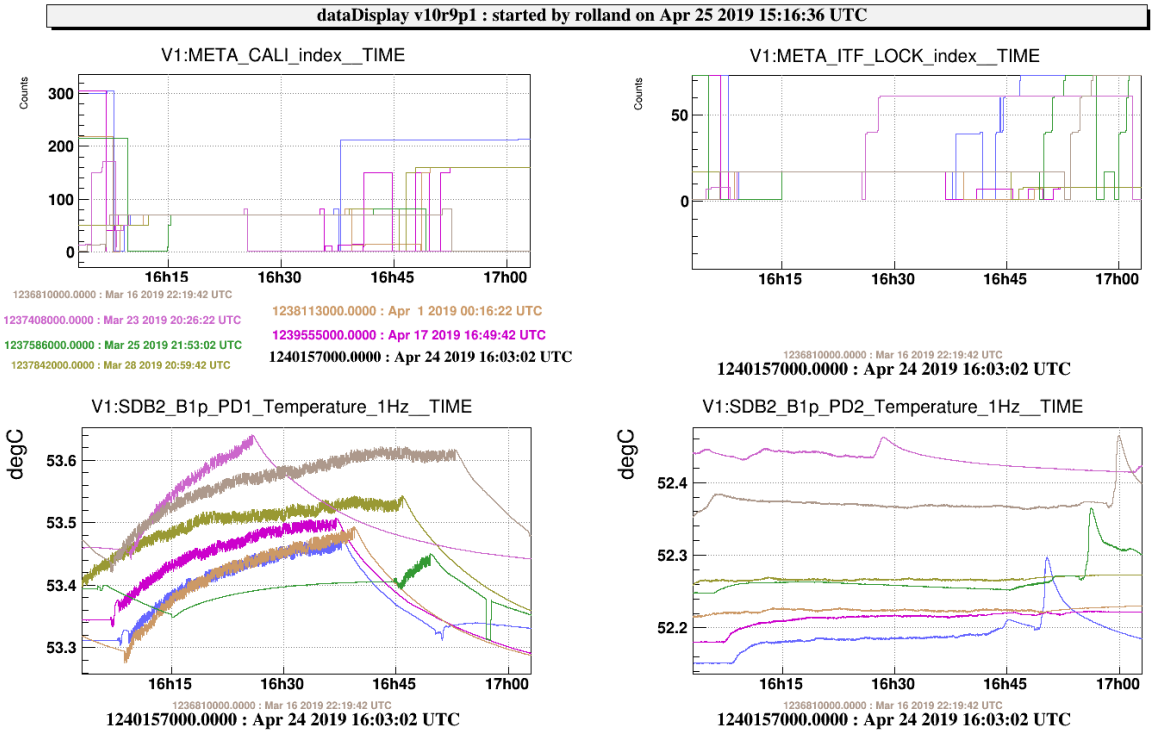

Figure 20: Temperature measured on the B1p photodiode preamplifiers during free swinging Michelson measurements. Top-left: state of the CALI automation node. Its value is around 70 during free swinging Michelson measurements. Top-right: state of the interferometer automation node. Its value is around 18 during free swinging Michelson measurements. Bottom: time series of temperatures of B1p PD1 (left) and PD2 (right).